Journal of Volcanology and Geothermal Research 460 (2025) 108279

Contents lists available at ScienceDirect

Journal of Volcanology and Geothermal Research

journal homepage: www.journals.elsevier.com/journal-of-volcanology-and-geothermal-research

Seabed stability inferred from the 2019–2020 earthquake swarm under a volcanic cone field and slopes of Condor Seamount, Azores

Neil C. Mitchell [a,*], Fernando Tempera [b,1], Thomas A. Morrow [c], Joaquim Luis [d], Christian Hübscher [e], Telmo Morato [f]

[a] Department of Earth and Environmental Sciences, University of Manchester, Williamson Building, Oxford Road, Manchester, M13 9PL, UK
[b] Instituto de Investigação em Ciências do Mar – Okeanos, Universidade dos Açores, Horta, Portugal
[c] NOAA Ocean Exploration, Oceanic and Atmospheric Research, National Oceanic and Atmospheric Administration, 1315 East West Hwy, Silver Spring, MD 20910, USA
[d] Universidade do Algarve, Portugal
[e] Institute of Geophysics, University of Hamburg, Germany
[f] Institute of Marine Sciences - Okeanos, University of the Azores, Horta, Portugal

ARTICLE INFO

Keywords:
Paleoseismology
Azores
Submarine landsliding
Multibeam sonar

ABSTRACT

Knowledge of the strength of submarine volcaniclastic deposits is important for assessing the stability of slopes of such materials and their geohazards but is difficult to measure. An opportunity for an alternative evaluation has been presented by an earthquake swarm under a volcanic seamount in the Azores. Attenuation relationships applied to earthquake data suggest that a cone field and flanks of the seamount experienced horizontal accelerations of >0.3 g during the swarm. However, multibeam sonar data collected before and after the swarm suggest that no slope failures occurred. Furthermore, in backscatter data collected after the swarm, low intensities below slopes suggest that muddy aprons were undisturbed by landslide debris. The swarm overlies cones with slopes near typical repose angles of non-cohesive particles. During earthquake shaking, the direction of maximum acceleration deviates from that due to gravity alone. We show that cone slopes effectively experienced much steeper gradients than their repose angles during the swarm. As they survived the shaking without failing, they were effectively stronger than non-cohesive sediment. We use a pseudo-static analysis to investigate the implied sediment strength, finding a ratio of undrained shear strength to vertical stress of >0.4–0.5. This implies shear strength of >24–30 kPa at 10 m depth below seabed. We speculate that carbonate cements and/or compaction may be responsible. If shallow areas are more widely strengthened, slope failure may then be less likely during moderate (M_L ~ 4.0 or less) seismic shaking and hence be less hazardous than if the slopes comprised wholly non-cohesive materials.

1. Introduction

Earthquakes can affect the geomorphology of the seabed, such as by causing slopes to fail (Morgenstern, 1967; Schwab and Lee, 1988; Hampton et al., 1996; Lee et al., 2009), which in turn can have other impacts, such as undetermined effects on biodiversity conditions and distribution. Some slopes of non-cohesive clastic sediment in subaqueous earthquake-prone environments have been observed to have slopes shallower than the typical angle of repose, which may be a sign of particle runout under the influence of earthquakes (Lee et al., 1994). Transponder-navigated submersible dive data from the Mid-Atlantic Ridge have revealed fault talus ramps with gradients of 27.5° (Mitchell et al., 2000) and submarine volcanic cones typically have slopes close to ~30° (Mitchell et al., 2012; Mitchell, 2021). These gradients are less than average gradients of subaerial scree slopes, which vary from ~33° to 35° (Tinkler, 1966; Chandler, 1973; Wallace, 1977; Akerman, 1984).

Giant landslides in volcanic islands have attracted attention because of their scale (Moore et al., 1989; Moore et al., 1994; Watts and Masson, 1995; Watts and Masson, 2001; Masson et al., 2002; Schindelé et al., 2024) and because the tsunamis that they generate potentially affect remote coasts (Ward and Day, 2001). In contrast, small submarine

* Corresponding author.
E-mail address: neil.mitchell@manchester.ac.uk (N.C. Mitchell).
[1] Present address: Unité Biologie des Organismes et Ecosystèmes Aquatiques (BOREA), Sorbonne Université, Muséum National d'Histoire Naturelle, Université de Caen Normandie, Université des Antilles, CNRS, IRD, Paris, France.

https://doi.org/10.1016/j.jvolgeores.2025.108279
Received 12 July 2024; Received in revised form 10 November 2024; Accepted 21 January 2025
Available online 27 January 2025

landslides (<10^8 m^3), which are common in the uppermost submarine slopes of volcanic islands (Chiocci et al., 2008a; Chiocci et al., 2008b; Mitchell et al., 2008; Casalbore et al., 2011; Quartau et al., 2014; Casalbore et al., 2015; Chang et al., 2021), have received almost no attention. The tsunamis they generate are potentially a significant threat also, despite their smaller size, because they are likely far more frequent (Kauahikaua et al., 1993; Chang et al., 2021; Chang et al., 2023). Tsunami runups may also be large because of proximity of adjacent coasts (Omira et al., 2016). For example, a 10^7 m^3 submarine landslide of Stromboli in 2002 produced runups of 10 m and caused extensive coastal damage to Stromboli and adjacent islands (Tinti et al., 2005; Tinti et al., 2006). (For comparison, landslide scars in the upper slopes of the central Azores islands have typical volumes of 10^4–10^6 m^3, though some reach 10^8 m^3 (Chang et al., 2021).) Although historical tsunamis within the Azores have been mainly attributed to earthquakes, 20–30 % are difficult to associate with earthquakes (Andrade et al., 2006) and may have been generated by submarine landslides. Quantifying the hazards from submarine landslides around volcanic islands remains a challenge, though.

Obtaining geotechnical data from these settings for slope stability analysis is difficult as sampling volcaniclastic slope material by devices such as Vibracorers are needed but cores from such materials are usually disaggregated and unsuitable for geotechnical analysis. Slopes around some landslide scars in the Azores reach 60°, which is much steeper than the ~30° angle of repose and suggests that they are stronger than non-cohesive sediment (Chang et al., 2021). Perhaps such volcaniclastic slope deposits are initially compacted and strengthened by seismic shaking (Sawyer and DeVore, 2015; ten Brink et al., 2016; Chang et al., 2021). Carbonate crusts are visible at the surface in east Condor Seamount (Fig. 1). Carbonate may also precipitate and form cements in the subsurface where carbonate-saturated ocean waters are forced into the seabed by ocean pressure fluctuations due to surface waves, tides and internal waves, and by the recharge components of geothermal circulation (van der Kooij et al., 2010; Tucker et al., 2020). Cements may be important for stabilising submarine slopes (Tucker et al., 2020) also, although it is unclear how far such stabilising cements continue below the seabed.

Paleoseismology is also challenging in submarine environments, where the seabed is obscured from satellite-based sensors. Fault ruptures have rarely been associated with individual earthquakes (Armijo et al., 2005; Escartín et al., 2016; Hughes et al., 2023; Leclerc et al., 2024), making it difficult to draw more general information from in situ observations. Morphologic dating (Arrowsmith et al., 1998) is unreliable underwater, as sediment movements do not follow the kinds of simple rules as creeping soils (Mitchell, 1996a). Dating fault scarps by luminescent methods (Gray et al., 2015) is not possible without exposure to light and is therefore limited to shallow depths only. Turbidity currents triggered by earthquakes have been inferred from turbidites shown by sediment dating to have been emplaced down different channels simultaneously, implying widespread failure expected of earthquake shaking (Adams, 1990; Goldfinger et al., 2003; Nieminski et al., 2024). Dating turbidites is a potentially powerful approach, but limited by the effort required to collect the cores and analyse them for paleoseismological events (Nieminski et al., 2024). Other ways to associate seabed changes with earthquakes, such as landslides, could therefore still be useful. However, seabed sediments and rocks vary enormously in strength, making interpretation of past landslide occurrences difficult without detailed in situ geotechnical data. To support such efforts, studies of morphological changes during known earthquake occurrences may be helpful.

A seismic swarm occurred on the west side of Condor Seamount near Faial Island in 2019 until early 2020. This allows us to investigate, using multibeam sonar data collected before and after the swarm, whether there were any seabed morphological changes associated with it. The results suggest that no slope failures occurred, despite peak horizontal accelerations exceeding 0.3 g. Submarine volcanic cones are produced by eruptions of particles from central vents, which typically are deposited nearly at the angle of repose (Mitchell et al., 2012). Where active cones have been studied and their formation from particles confirmed by vent observations (Chadwick et al., 2008a), landslide scars representing 50–100 m of erosion have been found in time-separated multibeam sonar surveys (Chadwick et al., 2008b) but we show that no such deep landslides occurred at Condor Seamount through the 2019–2020 swarm. Following the interpretations of the sonar data, we explore whether the seismic shaking should have strongly mobilised the slopes of cones and flanks of Condor Seamount if they were formed of purely non-cohesive volcaniclastic sediment. This leads us to conclude that the cones are stronger than expected for non-cohesive material and use a pseudo-static analysis to assess their effective strength.

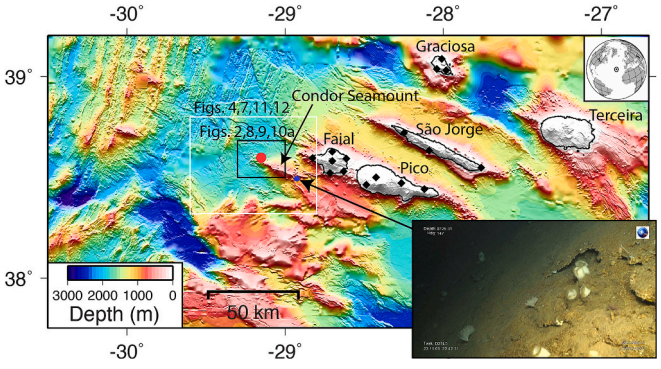

Fig. 1. Site of the 2019/2020 earthquake swarm over westerly Condor Seamount. Bathymetry is from the Global Multi-Resolution Topography (GMRT) synthesis grid (Ryan et al., 2009) (www.geomapapp.org), which largely comprises data from a cruise of RV *Le Suroit* in the study area (Luis et al., 2006). Black diamond symbols locate seismic stations on islands nearest to the swarm. Red circle is average location of the $M_L \geq 4.0$ events according to the earthquake catalogue studied here. Inset lower right: seabed at 725 m depth on east Condor Seamount revealing carbonate crusts (located by blue circle on main map). Photo courtesy of the EMEPC (https://en.emepc.pt/). Steepness of seabed is possibly exaggerated by camera tilt. (For interpretation of the references to colour in this figure legend, the reader is referred to the web version of this article.)

2. Background

Condor Seamount is a ridge lying immediately WSW of Faial Island (Fig. 1) on the Azores oceanic plateau (Gente et al., 2003). Its WNW-ESE orientation is similar to those of faults and other ridges of volcanic origin amongst the Azores central islands (Ligi et al., 1999) and is similar to the orientations of rifts and aligned cinder cones on Faial, Pico and São Jorge islands (Madeira and Brum da Silveira, 2003; Madeira et al., 2015). It therefore similarly developed from volcanism within this broad transtensional area between the African and Eurasian tectonic plates (Freire Luis et al., 1994; Lourenço et al., 1998; Vogt and Jung, 2004; Marques et al., 2013; Neves et al., 2013; Miranda et al., 2014; Miranda et al., 2015; Mitchell et al., 2018; Romer et al., 2018). Only one igneous sample recovered from Condor Seamount has been dated (Ar—Ar) as 1.10 ± 0.80 Ma (Beier et al., 2015). The full age extent of igneous activity at the seamount therefore remains an open question.

Bathymetry maps derived from multibeam sonar data (Fig. 2) reveal the elongated form of Condor Seamount, with a summit reaching to 184 m depth and a relief of ~1700 m above the surrounding seafloor. The flanks of the seamount contain shallow downslope-oriented ridges and valleys. In the west end of the seamount, a field of rugged conical features and small ridges can be observed. The small ridges are also oriented WNW-ESE. To characterize biological habitats, acoustic backscatter and seabed photographs have been studied extensively (Tempera et al., 2012; Tempera et al., 2013). These reveal high backscattering intensities over the seamount summit, corresponding with

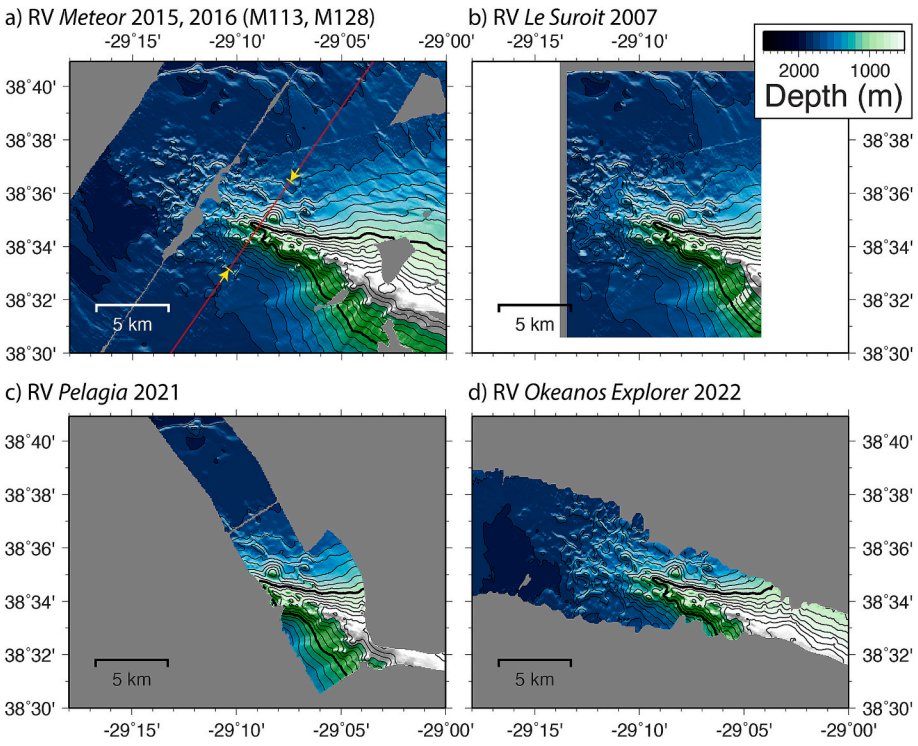

Fig. 2. Multibeam bathymetry maps centred on the earthquake swarm from before (a, b) and after the swarm (c, d). Map extent in Fig. 1. Contours are every 100 m, with 1000 m in bold. Yellow arrows on red line in (a) locate the extent of the seismic reflection profile in Fig. 3. (For interpretation of the references to colour in this figure legend, the reader is referred to the web version of this article.)

rocky outcrops, gravels and boulders. The boulders are well-rounded, suggesting that the summit has been influenced by surf during one or more Pleistocene glacial lowerings of sea-level. As the 184 m shallowest depth lies beneath the Pleistocene low-stands (~120 m (Bintanja and van de Wal, 2008)), the seamount has subsided since its formation (Tempera et al., 2012). Seabed photographs over the mostly smooth flanks of the seamount reveal both unconsolidated sediment and sediment that had been made rigid by carbonate cements. On the north flank, sediment is mainly bioclastic down to 965 m, below which it is black volcaniclastic with silt- and clay-grade particles (Zeppilli et al., 2013). Modelled currents reach only a modest 0.1 m/s (Mohn et al., 2023) and current meters have recorded similar 0.1–0.2 m/s (Bashmachnikov et al., 2013).

No seabed photographs are available from the cone field at the westerly end of the seamount. However, one seismic profile crossing it (Romer et al., 2018) reveals internal reflections that are sub-parallel to the seabed as would be expected from growth of each cone from particles erupted from central vents (Chadwick et al., 2008a). Fig. 3 shows an enlargement of one of the profiles, revealing the laterally uniform character of the dipping reflections from within four structures, which have been interpreted as formed from volcaniclastic deposits (Weiß et al., 2015). Disrupted reflections around a cone summit and possible vent can also be observed ("S" in Fig. 3). The contrast in morphology from rugged cone field at the end of Condor Seamount to smooth flanks around its waist is reminiscent of that found at Hawai'i Island (Smith et al., 2002). There, the submarine Puna Ridge is rugged, a result of wholly submarine eruptions, whereas the steep submarine slope adjacent to the East Rift Zone is smooth, a result of flows of clastic particles formed when lava has reached the sea (e.g., Fornari et al., 1979). The similar transition at Condor Seamount implies that the centre of the seamount formed with the summit near sea-level, leading to lava-seawater interactions that have left its flanks smooth (Tempera et al., 2012). Particles originating from shallow-water biogenic production may have also contributed (Tempera et al., 2013) and shallow-

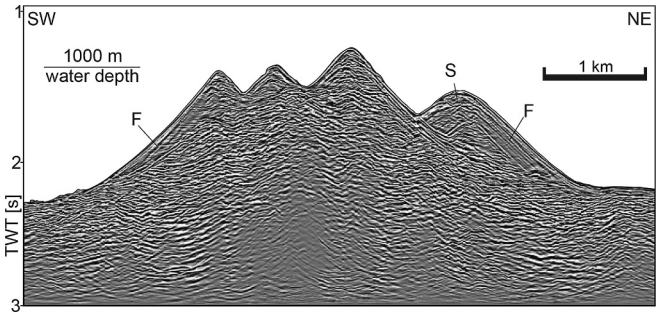

Fig. 3. Seismic reflection record from RV *Meteor* cruise M113/1 (Hübscher et al., 2015; Romer et al., 2018) crossing volcanic structures of NW Condor Seamount (located in Fig. 2a). Data were collected using signals from an array of four GI airguns recorded on a digital streamer of 600 m active length and 144 channels. These data were processed using standard methods (velocity analysis, moveout correction, frequency filtering). The data were also migrated, hence upward-curved trends are artefacts of the migration. The data were visualised using SeiSee software. Annotation: TWT, seismic two-way time, F, flank reflections, S, summit disrupted reflections. Horizontal bar is at 1.333 s TWT, i.e., 1000 m depth in the water column for seismic velocity 1500 m/s. Vertical exaggeration is 2:1.

penetration (15 cm) sediment cores from the seamount flanks have recorded largely bioclastic silty sand (Zeppilli et al., 2013). The emplacement of these deposits by many sedimentary flows originating from shallower water in turn implies that the flanks likely contain beds of varied geotechnical properties lying parallel to the seabed. Such configurations can be prone to failure (ten Brink et al., 2009). Indeed, some landslide scars can be identified in the detailed bathymetry (Tempera et al., 2013), although those scars have smooth side and head walls, suggesting they have been modified by more recent sediment deposits (Chang et al., 2021). Otherwise, the smooth morphology with small gullies imaged in the acoustic backscatter suggests that small

failures or sedimentary flows have mainly affected the flanks. Based on photographic evidence, Tempera et al. (2013) interpreted the seamount flank material as largely unconsolidated, and a 1-km-wide band over the summit as consolidated or cemented material. Similar extensive carbonate crusts have been reported on other seamount and islands slopes down to ~1 km depth (Tucker et al., 2020).

3. Data and methods

3.1. Earthquake data from the local seismometer network

Seismicity was recorded continuously by the Portuguese National network (IPMA) of broadband, enhanced short-period and some strong-motion sensors distributed amongst the Azores islands (Carrilho et al., 2021). Detection of individual events depends on earthquake size, distance to stations and local noise characteristics at those stations. However, based on the station distribution shown in Fig. 1, swarm events were likely mostly recorded by stations on Faial Island, and to varying extents on São Jorge, Terceira and Graciosa. From the station distribution, we might expect epicentre location uncertainty to be smallest in the NE-SW direction and largest in the NW-SE direction.

Two simple displays of the data were generated to illustrate the spatial and temporal progression of the swarm. Total seismic moment of events falling within cells of 0.01° X 0.01° (latitude X longitude) was computed and provided as a map. A polygon was traced by eye around the swarm (Fig. 4) and used to select swarm events. The cumulative change in total seismic moment encompassed by that polygon is shown in Fig. 5.

Cumulative and incremental frequency (Güttenberg-Richter) graphs were computed from local magnitudes (Fig. 6). From the change away from the linear trends of those graphs (the "magnitude of completeness"), the local network appears to have detected events of $M_L > 2.0$ well at this location.

For assessing the effects on the seabed, a map was computed of peak horizontal acceleration (PHA) induced by the earthquakes following a similar procedure to that of Chang et al. (2021). PHA within each grid cell of 0.01° X 0.01° was computed from horizontal distance to each event using the empirical relationship of Mezcua et al. (2008). This relationship was based on strong-motion recordings of earthquakes in Iberia of magnitude 3.0 to 5.3, overlapping magnitudes of swarm earthquakes in the IPM recordings. As the events are outside the network of recording stations on the islands, their depths are unreliable. A common 10 km depth was therefore set, somewhat shallower than the

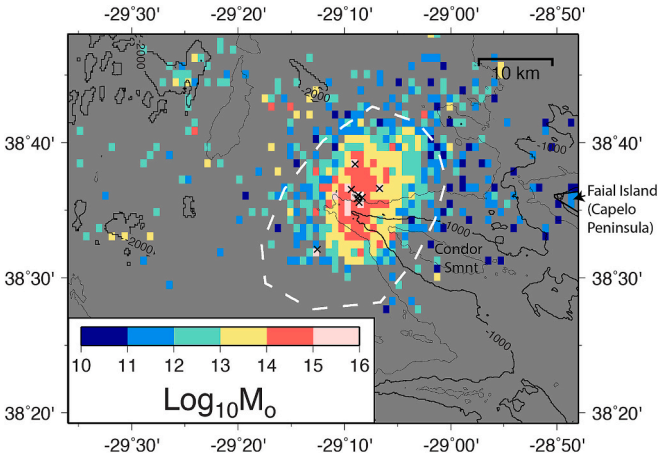

Fig. 4. Cumulative seismic moments for the period 2019/01/01 to 2020/07/15 (IPMA recordings). White polygon locates area of selected seismicity summarised in Figs. 5 and 6. Black contours are from the GMRT (Ryan et al., 2009) (shown every 500 m, with every 1000 m in bold; grid of April 2024). Cross symbols locate the events of $M_L \geq 4.0$ in the IPMA catalogue.

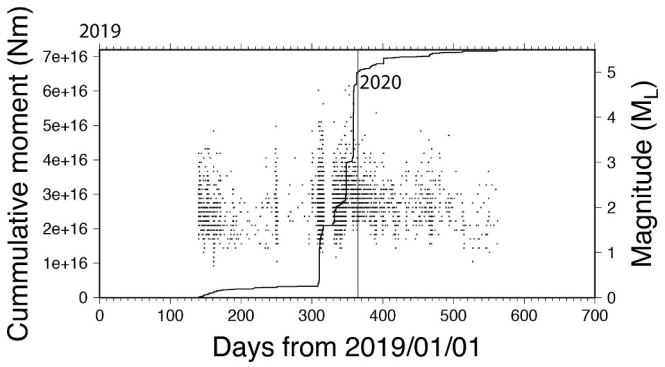

Fig. 5. Seismicity recorded by the IPMA within the polygon marked in Fig. 4. Solid line shows the cumulative seismic moment released and x-symbols are individual events (right-hand scale). Vertical line marks start of year 2020.

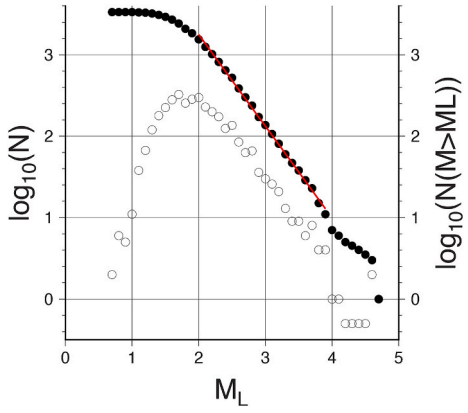

Fig. 6. Magnitude-frequency distribution for the selected IPMA data. Open circles show the incremental distribution in M_L (left-hand scale) and solid circles the cumulative distribution (right-hand scale). Red line shown is a least-squares regression, which suggests the swarm β-value was 1.126 ± 0.001. (For interpretation of the references to colour in this figure legend, the reader is referred to the web version of this article.)

average ~ 12 km depth of aftershocks of the 1998 earthquake east of Faial (Matias et al., 2007) due to Condor Seamount lying on younger crust and hence thicker lithosphere. The results in Fig. 7 are dominated by the events of $M_L > 4.0$ as would be expected. Carrying out the calculations instead with a common 12 km depth lowered the maximum PHA by 19 %.

The actual horizontal acceleration experienced at a particular location during a particular earthquake will also depend on the polarity of the shear wave at that location (which itself depends on the sense of movement on the fault plane, location of observation, etc.). This affects the extent to which the acceleration is down-slope, promoting failure. The Mezcua et al. (2008) analysis did not account for polarity, hence their equation represents the acceleration expected averaged over all azimuths. Nevertheless, the high PHA values in Fig. 7 are dominated by the eight $M_L \geq 4.0$ events. As they are widely distributed across the cone field, this implies varied azimuths of propagation of the seismic waves at any given location. The seabed should have experienced maximum accelerations that were broadly similar to these values.

3.2. Sonar and seismic reflection datasets

We have accessed the following multibeam data collected before and after the seismic swarm. Unfortunately, the details of data processing (e.g., where sound velocity profiles were taken and employed) are commonly missing, though some places have been surveyed multiple

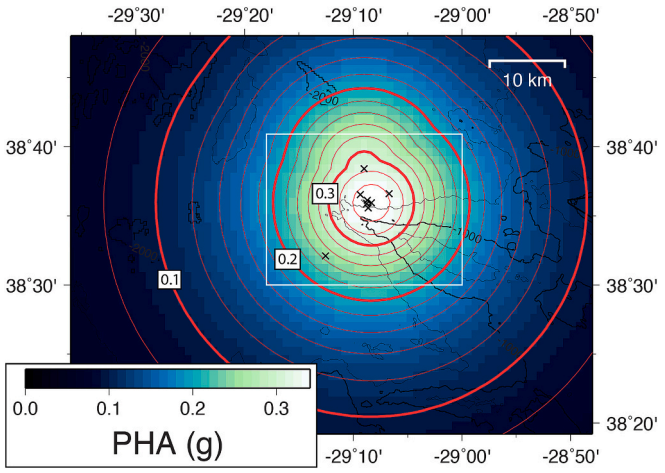

Fig. 7. Peak horizontal acceleration experienced during the period 2019/01/01 to 2020/07/15, estimated from the IPMA catalogue using the Mezcua et al. (2008) relation. Values are in fractions of g (acceleration due to gravity) and contours are every 0.02 g. White-outlined box locates Figs. 2, 9, 10 and 11a. Cross symbols locate events of $M_L \geq 4.0$ as Fig. 4. Black contours represent depths from the GMRT grid (Ryan et al., 2009) every 500 m, with 1000 m in bold.

times during different cruises before and after the swarm, which have allowed us to check for consistency. Artefacts in multibeam sonar data typically produce systematic and random errors parallel and perpendicular to vessel tracks with known characteristics (de Moustier and Kleinrock, 1986; Hughes Clarke et al., 1996; Mitchell, 1996b; Schmitt et al., 2008), which can be considered during interpretation. All data used here were collected during times of GPS availability.

Before the seismic swarm, data were collected over the swarm area with a 12 kHz Kongsberg EM122 multibeam system during RV *Meteor* cruises 113/1 in 2016 (Hübscher et al., 2016) and 128 in 2017 (Beier et al., 2017). It was also surveyed aboard RV *le Suroit* using a 30 kHz Kongsberg EM300 multibeam sonar in 2006–2007 (Luis et al., 2006; Miranda et al., 2014), from which we also have acoustic backscatter data.

Data were collected after the swarm in two surveys, exploiting transits to/from Faial Island. The first on RV *Pelagia* was carried out with a 30 kHz Kongsberg EM302 sonar in June 2021, for which we also have acoustic backscatter data. The second post-swarm survey occurred during a transit of the RV *Explorer* using a 26 kHz Kongsberg EM 304 sonar in September 2022. The survey report (Candio et al., 2022) indicates that sound velocity data used for refraction corrections were collected every four hours.

The multibeam sonar data vary in spatial resolution. Some data were supplied as individual soundings (*Meteor*, *Explorer*, *Pelagia*), whereas *le Suroit* data were provided in gridded form with 50-m cell size. Acoustic spatial resolution at the seabed equals $\theta.R$, where θ is beam width in radians and R is range (de Moustier, 1988). Hence, for vertical beams under the vessel track, a typical 1° beam width implies an acoustic resolution of 3 m at the 184 m depth of the summit of Condor Seamount and 44 m at 2500 m depth. To ensure a roughly comparable resolution between grids encompassing the coarsest of these data, all data were binned and regridded to a common 50-m cell size, which should also strongly reduce random errors.

The Towed Ocean Bottom Instrument (TOBI) (Murton et al., 1992; Flewellen et al., 1993) was deployed around the central Azores islands in 1999 (Ligi et al., 1999). The data were formed into mosaics by researchers at the Consiglio Nazionale delle Recerche in Bologna (Stretch et al., 2006; Mitchell et al., 2018), one of which is shown here for the westerly end of Condor Seamount and its summit. These data were collected with the instrument towed close to the seabed (~200–500 m) so they have higher resolution than most of the multibeam sonar data.

The sonars providing all four sets of acoustic backscatter were not acoustically calibrated and hence do not provide quantitative backscattering strengths (Mitchell and Somers, 1989). We therefore show the backscatter data only as gray-scale maps. Typically, contrasts in backscattering data are caused by varied seabed type (e.g., mud is low backscattering, whereas bare rock is high backscattering), though backscattering also varies with the angle of incidence of the signal with the seabed and hence with seabed topography (Mitchell and Somers, 1989). When sidescan sonar data are collected at low altitudes above the bed, such as TOBI here or the RV *Explorer* swath crossing the seamount summit, elevated objects (such as volcanic cones) cast prominent acoustic shadows. Further details on backscatter data interpretation can be found in Blondel and Murton (1997).

3.3. Assessment of stability for non-cohesive particles

As our analysis of the sonar data below suggests that there was no major failure in the volcanic cones and other steep slopes, we explore whether the seabed was effectively non-cohesive or cohesive with a simple test. During earthquakes, seabed particles experience a maximum acceleration from the gravitational field that is distorted by the horizontal accelerations. The direction of vertical (maximum acceleration direction) in the reference frame of the seabed depends on the polarity of the seismic shear waves, which will have varied with azimuth from each earthquake source. However, a rough indication of this tendency can be provided by simply adding arctan(PHA) derived from the grid in Fig. 7 to the local seabed maximum gradients of Fig. 8a, where PHA data are in fractions of g (the acceleration due to gravity). This will only represent the true distorted vertical effect in parts of the area where the S-wave polarity was optimal (i.e., accelerations in the down-slope direction). Nevertheless, the eight events of $M_L \geq 4.0$ are spread about the central area. Optimal polarities can be expected from each of them in different areas, in aggregate covering much of the central area. The vertical accelerations are ignored by this analysis, as they have less distorting effect on the maximum acceleration direction if they are only a fraction of g.

3.4. Assessment of seabed strength

The effective strength of slope materials was then investigated using the pseudo-static equation of Morgenstern (1967):

$$\frac{S_u}{\sigma'_v} = 0.5 sin(2\alpha) + k\frac{\gamma}{\gamma'} cos^2(\alpha) \quad (1)$$

Although we do not anticipate the cones to be cohesive in same sense as compacted mud, the objective is to estimate S_u as a proxy for strength to get a sense of its magnitude for comparison with other measurements. Eq. (1) provides the ratio at the point of failure of minimum S_u (peak undrained shear strength at a level of potential failure within the seabed) to σ'_v (the vertical stress at that level due to overlying sediment, allowing for the effect of buoyancy in water). The other values are: α, the local bed gradient, k, PHA (in fraction of g), γ, the sediment unit weight and γ' the sediment unit weight in water (i.e., buoyancy-corrected). The construction of Eq. (1) ignores the effects of cyclic loading, transient pore pressure changes, vertical seismic accelerations and other factors (Morgenstern, 1967; ten Brink et al., 2009). In particular, soil weakening is progressive, hence they are likely to be weakest during later parts of an earthquake's coda, occurring after the peak acceleration (Rampello et al., 2010). To account for such effects, Rampello et al. (2010) inserted a further dimensionless parameter η (with values 0–1) before k. In their application of this equation to the seabed around Iberia, Collico et al. (2020) used $\eta = 0.25$ of Rampello et al. (2010) for soft-medium soils and PHA of 0.1–0.2 g. (For context, the value η varies ~0.1–0.5 between different soils, earthquake magnitudes and displacements in Rampello et al. (2010).) Note also that the first term in Eq. (1) reaches a maximum when α approaches 45°, suggesting a limitation of this approach. In

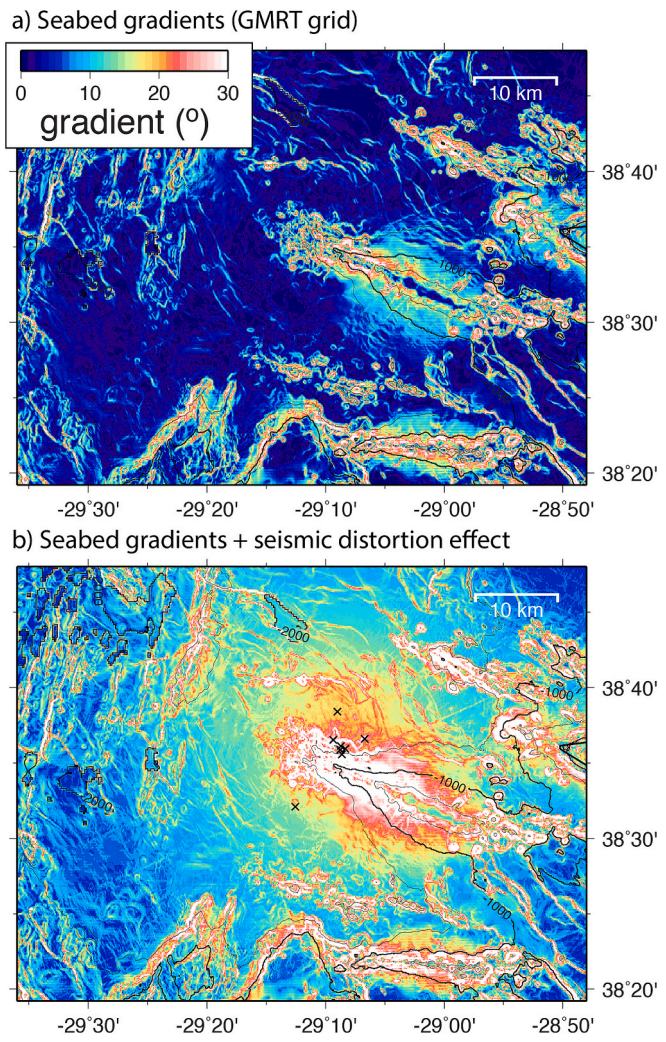

Fig. 8. (a) Seabed gradient angles (local maxima) computed from the GMRT grid, which largely consists of *Le Suroit* multibeam data over the area of interest. (b) The gradients of (a) with arctan (PHA) in degrees from Fig. 7 added to the seabed gradient. Cross symbols locate events of $M_L \geq 4.0$ as Fig. 4. Bathymetry contours in both panels are from the GMRT (Ryan et al., 2009).

practice, the cone slopes reach ~30°, so this is mostly not a problem in this study, but the method will be less useful for steeper slopes.

To explore slope rigidity at scales larger than the small volcanic cones, values for α were computed from the GMRT (Ryan et al., 2009) after filtering the grid with a 2-km-wide cosine-tapered filter (the GMRT here mostly comprises *Le Suroit* multibeam-derived depth data). Another set of calculations was carried out without filtering, with a grid cell size of 50 m. Values of k are from the grid shown in Fig. 7 and $\eta = 0.25$. As we have no reliable sediment density data locally, we used a bulk density (γ) of 1600 kg/m^3 as a typical value for core 6G of Winters and Lee (1982), which contained half sand-grade material and was recovered from carbonate-rich sediments. (If 1500 and 1700 kg/m^3 are used for γ, the resulting maximum S_u/σ'_v ratio increases by 9 % and decreases by 6 %.)

4. Observations

4.1. Seismicity and ground motions

Earthquakes occurred under the volcanic cone field of the NW end of Condor Seamount (Fig. 4), forming a NE-SW-oriented band that likely reflects event location uncertainties. Its centre lies roughly around the 1500 m depth contour on the north flank. The swarm occurred over ~500 days, initiating with ~150 days of modest seismic moment release (Fig. 5). Subsequently, most of the seismic moment was released in 2–3 phases towards the end of 2019 in less than 100 days, following ~150 days of modest release. The largest-magnitude events occurred during these most intense 100 days and the largest events had comparable magnitude ($M_L \sim 4.7$). The magnitude-frequency graphs (Fig. 6) each contain a linear segment. Fitting a line through the linear segment in each case suggests a β-value of −1.13 above $M_L = 2.0$. Above $M_L = 4.0$, the graphs flatten out, breaking the power-law trend, reflecting the various higher magnitude events recorded (Fig. 5).

4.2. TOBI sidescan sonar imagery

We update previous reporting of these data (Mitchell et al., 2018), focusing on west Condor Seamount (Fig. 9). The data are useful for confirming the presence of small features such as cones in the multibeam data. The TOBI images reveal moderately high backscattering over the summit of Condor Seamount, with small elongated cones in its upper flanks, which cast deep acoustic shadows. Towards the NW end of the summit, the truncated cone marked in Fig. 9 has downslope-trending high and low backscatter features on its west side, which are interpreted here as caused by the deposits of sedimentary flows of clastic particles. The "smooth cone" north of it also likely formed from eruptions of particles from a central vent. (Repeated emplacements of particles led to the laterally uniform seismic reflections in the profile shown in Fig. 3 (feature "S"), which was collected running across the NW flank of this cone (Fig. 2a).) Further to the NW, the series of small ridges observed in the multibeam bathymetry correspond with high backscattering lineaments in the TOBI imagery. In this cone field, acoustic backscattering varies greatly over short lengthscales (<1 km), suggesting the presence of rock outcrops interspersed by mud. Some dark patches are the result of acoustic shadows cast by elevated features.

4.3. Apparent changes in bathymetry

Differences between the bathymetry grids of Fig. 2 are shown in Fig. 10. Superficially, these appear to indicate accretion (positive elevation change) and erosion (negative) but we show later that all can be explained as artefacts. Feature 'a' (Fig. 10c) is a broad area of positive change corresponding to deep bathymetry in Fig. 2b and is absent from Fig. 10a. At 'b' (Fig. 10b and d), the bathymetry appears to have become generally deeper in the *Explorer* data on the north side of Condor Seamount and shallower by a similar amount on the south side of the seamount. Positive features 'c' and 'd' correspond with sharp steps observable in the grids in Fig. 2 and have different locations between Fig. 10b and d. Localised positive features 'e' lie at the edges of contributing swaths. Negative feature 'f' (Fig. 10a) corresponds to a small hill in the *Meteor* data and is absent in Fig. 10c. Negative feature 'g' (Fig. 10c) is absent in Fig. 10a.

4.4. Acoustic backscattering

We do not explore changes in backscattering, as this would require coincident survey lines, etc., but instead observe some aspects of backscatter data collected after the swarm. Fig. 11b and c both show lower backscattering ("L") in the lower flanks of Condor Seamount, with abrupt transitions at ~1100 m depth. Small gullies on the south side are associated with bands of low backscattering in Fig. 11c. Around the base of the smooth cone in both figure panels (south, east and NW), backscattering is low.

5. Interpretations of apparent bathymetric changes

The above-described features appear to be all explainable as bathymetric artefacts, originating from the different survey platforms, survey geometries and methodologies used. Feature 'a' is most likely to have

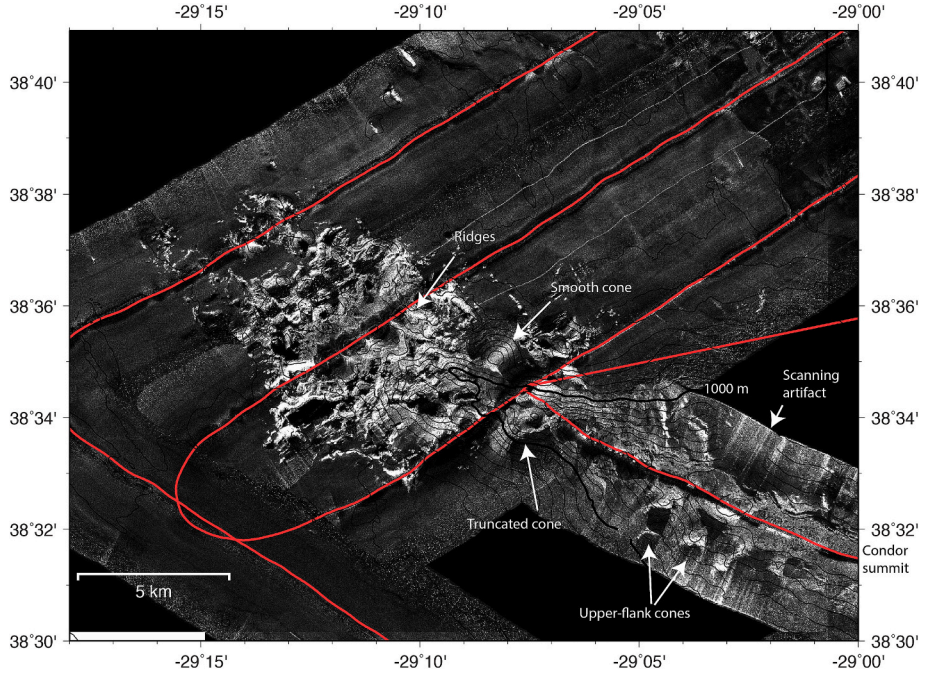

Fig. 9. Towed Ocean Bottom Instrument (TOBI) sidescan sonar mosaic of the cone field and westerly Condor Seamount (data from Ligi et al. (1999) and Mitchell et al. (2018)). White tone represents high backscatter. Red Lines are tracks of the TOBI vehicle. Bathymetry contours are from Fig. 2a. (For interpretation of the references to colour in this figure legend, the reader is referred to the web version of this article.)

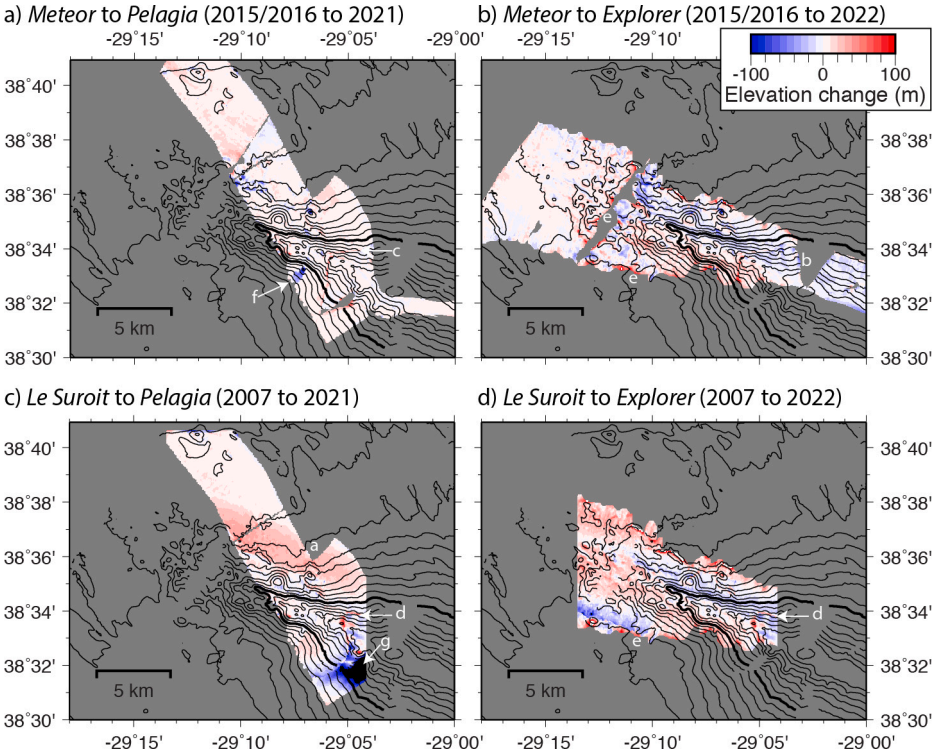

Fig. 10. Apparent changes in seabed elevation implied by different multibeam data collected before and after the swarm (elevation after minus elevation before the swarm). Bathymetry contours (every 100 m, 1000 m in bold) are from the RV *Meteor* grid. Annotations 'a' to 'g' locate changes that can be explained as artefacts of data collection or processing (see main text). Bathymetry contours are from Fig. 2a.

been caused by a sound velocity correction error. A difference in positioning explains feature 'b' (also note similar apparent depth changes in the small ridges to the WNW in the cone field), if the *Explorer* data were misplaced to the north by ~20–30 m. Features 'c' and 'd' are errors where different grids appear to have been combined. Features marked 'e' are due to data from beams near the outer edges of swaths, which are typically noisier due to weaker backscattered signals.

Features 'f' and 'g' are interesting as they have morphologies expected of geological changes. Feature 'f' appears as though a block was removed during the swarm. However, it does not appear in Fig. 10c and

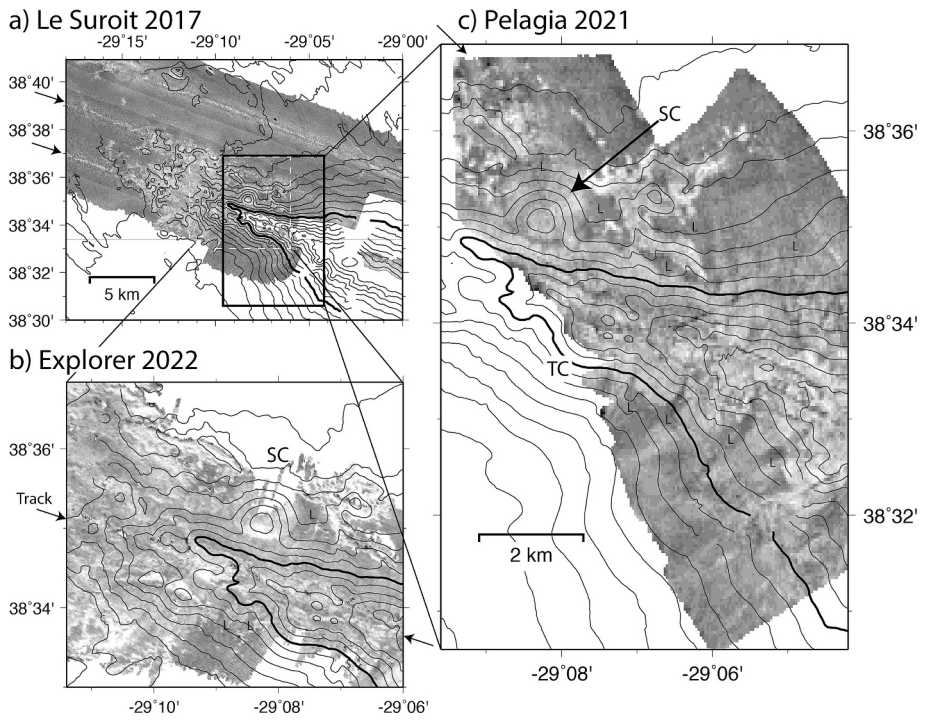

Fig. 11. Acoustic backscatter maps produced from data collected (a) before and (b, c) after the earthquake swarm. Higher backscatter is represented by lighter tones. Areas without data are white. Small arrows locate ship tracklines. Annotation: L, low-backscattering at base of slopes and in gullies, TC, truncated cone, SC, smooth cone (Fig. 9). Solid and dashed-white rectangles in (a) locate the maps in (b) and (c), respectively. Bathymetry contours are from Fig. 2a.

the backscatter image collected after the swarm (Fig. 11b) shows no evidence for it (backscattering is uniformly low beneath this feature, not high as would be expected from removal of superficial muds). Based on the lack of corresponding backscatter evidence, we suspect this is a sounding artefact indistinguishable from similar-shaped geologic structures at this resolution and was left in the dataset when gridded. The apparent landslide 'g' also coincides with low backscattering in Fig. 11b. Along with its absence in Fig. 10a, this feature also seems likely to be an artefact.

The low backscattering around the base of the smooth cone (Fig. 11b and c) is suggestive of low-backscattering mud sufficient to attenuate the signals from any underlying rocky surface. At the 26–30 kHz frequencies, attenuation in muds is ~1 dB/m and leads to complete loss of backscatter at 15° grazing angle if the mud is >1 m thick (Mitchell, 1993). The data suggest that these and other low-backscattering areas lying beneath slopes have not been over-lain by debris from landsliding and remained muddy.

In conclusion, no major change occurred during the swarm. Attributing uncertainties to this statement is difficult, given the varied quality of the multibeam data and as acoustic resolution varies greatly with water depth and across-swath. Based on the variations in Fig. 10 and considerations above, we suggest that a depth change of 50 m over a lengthscale of 1 km should be resolvable in these data and perhaps smaller given the redundancy of multiple surveys. Any bathymetry changes were smaller than this. Smaller slope failures are also unlikely given the undisturbed low-backscattering mud around the smooth cone and lower seamount slopes.

6. Discussion

The lack of a main shock and the occurrence of multiple events of similar magnitude (M_L) > 4.0 during the Condor swarm (Fig. 5) are typical of volcanic earthquake swarms (McNutt, 1996; Pritchard et al., 2018; Tepp and Dziak, 2021). Volcanic swarms can have steep magnitude-frequency graphs, with extreme β-values reaching 3.0, though some much lower (McNutt, 1996). The modest 1.13 β-value found for Condor Seamount (Fig. 6) is within the range for volcanic swarms, though not diagnostic of such swarms. At present, we interpret this swarm as either tectonic or volcanic involving only small magma volume and hence small dike opening. The sonar data rule out an eruption at the seabed during the swarm within the surveyed areas. We devote the rest of the discussion to addressing the strength of the seabed sediments implied by the lack of significant landsliding observed.

6.1. Would seismic accelerations have mobilised non-cohesive sediment?

If the slopes comprised non-cohesive sediment, we might expect to have observed morphological changes comparable to the 50–100 m scars that were found at the Monowai active submarine volcano (Chadwick et al., 2008b), as well as evidence for the debris transported by them where instead we observe low-backscattering muddy aprons. Slopes of non-cohesive particles can be irregular at small scale due to local support amongst irregularly shaped particles, as illustrated by laboratory experiments attempting to replicate threshold hillslopes (Densmore et al., 1997). Despite that irregularity, however, those experiments illustrate how failure in such material can clear whole slopes, leaving them remaining near the angle of repose, as typically observed in submarine scree slopes (Mitchell et al., 2000). Consequently, large failures may not always be so obvious from morphology, though should be revealed from changes in bathymetry and from disrupted deposits around them.

The sum of seabed gradient and arctan(PHA) in Fig. 8b lies well above 30° in large areas of steep slopes around the western end of Condor Seamount, its flanks and the slopes of the cone field. The maximum is 73°. The distorting effect of horizontal accelerations therefore suggests that materials would have been mobilised if they had been non-cohesive. As we observe no evidence for mobilisation in the multibeam bathymetry and in the after-swarm backscatter (Fig. 11b), such movements, if they occurred, were too small to be detected in these data. Some clastic sediment may be secured by consolidated by earlier

shaking by earthquakes (Sawyer and DeVore, 2015; ten Brink et al., 2016) and/or carbonate cementation as speculated earlier to explain steep landslide headwalls (Chang et al., 2021).

6.2. Constraints on the effective cohesive seabed shear strength

The results of applying the modified Morgenstern (1967) equation in Fig. 12 suggest that some areas in the cone field resisted shaking with S_u/σ'_v ratio of >0.4 (regionally filtered bathymetry) or > 0.5 (unfiltered bathymetry). The minimum S_u values can be estimated from these ratios by using the 1600 kg/m^3 bulk density to estimate σ'_v. The vertical stress at 10 m depth below seabed would then be 60 kPa (allowing for buoyancy), hence, S_u should be at least 24–30 kPa. For comparison, these S_u values lie within the range of measured values for carbonate ooze and somewhat larger than <20 kPa for siliciclastic sediments (Kenter and Schlager, 1989).

6.3. Implications for hazards analysis

If the mechanisms strengthening the Condor Seamount slopes also apply to the upper submarine slopes of the Azores islands, those slopes should also be safer from shaking by earthquakes of similar M_L ~ 4.0–4.7 than would be otherwise. Earthquakes are frequent and widespread amongst the islands (Madeira et al., 2015), so the consolidation mechanism (Sawyer and DeVore, 2015; ten Brink et al., 2016) may apply. The precipitation of carbonates is widespread in shallow waters of the Azores, where the water is supersaturated for aragonite (Wisshak et al., 2015), so the cementation mechanism (van der Kooij et al., 2010; Tucker et al., 2020; Chang et al., 2021) may also apply more generally. The lack of deep failures on Condor Seamount would be consistent with cementation occurring deep within the seabed. The finding that no major landslides were triggered by the earthquake swarm on Condor Seamount is a promising development as it may imply that the island slopes are also broadly stable to moderate shaking. However, if the island slopes are not mobilised by moderate shaking, this may allow slope deposits to thicken over time, which may therefore be susceptible to larger-scale failure when affected by more extreme shaking (Chang et al., 2021).

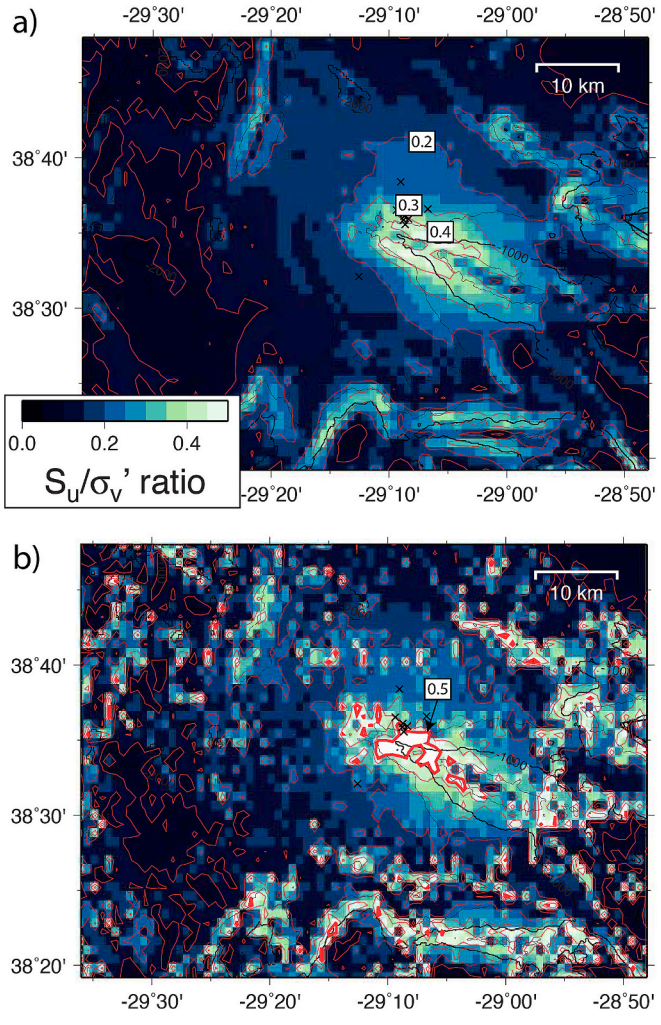

Fig. 12. Minimum estimates of the ratio of effective undrained shear strength to vertical stress obtained from the relation of Morgenstern (1967) (Eq. (1)). Contours are every 0.1. Cross symbols locate events of $M_L \geq 4.0$ as Fig. 4. Bathymetry contours are from the GMRT (Ryan et al., 2009). (a) Calculation after filtering the bathymetry grid over 2-km scales and (b) calculation without filtering.

7. Conclusions

Bathymetry data collected before and after the 2019 earthquake swarm have allowed us to investigate whether any changes of the seafloor occurred at Condor Seamount. Although these data may not reveal small movements, no major landslides were detected. Furthermore, low backscattering around the base of a central cone and the slopes of Condor Seamount in data collected after the swarm suggests the presence of mud that was not disturbed by landsliding or landslide debris. The apparent stability of these slopes was investigated in two ways. First, the distortion of the locally felt vertical direction was assessed by simply adding arctan(fractional peak horizontal acceleration) to the local maximum gradient. The result is only correct in parts of the area, as it ignores the seismic wave polarity, but shows that some oversteepening effects should have occurred. As no failures were detected, this implies that the bed was effectively not non-cohesive. Second, we assessed seabed strength by computing the ratio of undrained shear strength (S_u) to vertical stress using a pseudo-static assumption. The result suggests that this ratio reached 0.4–0.5. For sediment at 10 m depth, this implies S_u > 24–30 kPa, equivalent to a somewhat strong marine sediment. These volcaniclastic sediments may have been strengthened by compaction aided by repeated shaking by previous earthquakes and by precipitation of carbonate cements. As such mechanisms likely apply to shallower waters around the islands also, the uppermost slopes of the islands may be similarly stable under moderate shaking by earthquakes of similar M_L 4.0–4.7. Although the hazards from larger-magnitude earthquakes are still a concern, this is a promising development, implying a lower risk of tsunami from submarine slope failure triggered by moderate earthquakes.

Funding

This work was partly supported by the Natural Environmental Research Council, UK (research grant NE/T014814). The RV *Pelagia* ship-time was provided free of charge as part of the iMAR project which received funding from the European Union's H2020 Research & Innovation Programme under grant agreement No 824077 EUROFLEETS+ (Telmo Morato principal investigator).

CRediT authorship contribution statement

Neil C. Mitchell: Writing – review & editing, Writing – original draft, Visualization, Software, Methodology, Investigation, Formal analysis, Conceptualization. **Fernando Tempera:** Writing – review & editing. **Thomas A. Morrow:** Writing – review & editing, Investigation, Data curation. **Joaquim Luis:** Writing – review & editing, Data curation. **Christian Hübscher:** Writing – review & editing, Data curation. **Telmo Morato:** Writing – review & editing, Data curation.

Declaration of competing interest

The authors declare that they have no known competing financial interests or personal relationships that could have appeared to influence the work reported in this paper.

Acknowledgements

We thank the officers and crews of the research vessels involved in collecting the marine geophysical data shown here. We thank Fernando Carrilho for the IPMA seismicity data used in this article. The Portuguese Task Group for the Extension of the Continental Shelf (EMEPC) and project CORALFISH (FP7ENV/2007/1/213144) is acknowledged for sharing seabed imagery from remotely-operated vehicle (ROV) dives on Condor including the photo in Fig. 1. Most figures were created using version 4.5.8 of the free GMT software system (Wessel and Smith, 1991; Wessel et al., 2019). We thank editor Ed Llewellin, reviewer Daniele Casalbore and an anonymous reviewer for their comments, which prompted a revision of the stability analysis and other changes. Any use of trade, product, or company names is for descriptive purposes of the methodology used only and does not imply endorsement by NOAA or the US Government.

Data availability

The authors are unable or have chosen not to specify which data has been used.

References

Adams, J., 1990. Paleoseismicity of the Cascadia subduction zone: evidence from turbidites off Oregon-Washington margin. Tectonophysics 9, 569–583.
Akerman, H.J., 1984. Notes on talus morphology and processes in Spitsbergen. Geogr. Ann. 66A, 267–284.
Andrade, C., Borges, P., Freitas, M.C., 2006. Historical tsunami in the Azores archipelago (Portugal). J. Volcanol. Geotherm. Res. 156, 172–185.
Armijo, R., Pondard, N., Meyer, B., et al., 2005. Submarine fault scarps in the Sea of Marmara pull-apart (North Anatolian Fault): Implications for seismic hazard in Istanbul. Geochem. Geophys. Geosyst. 6, Q06009.
Arrowsmith, J.R., Rhodes, D.D., Pollard, D.D., 1998. Morphologic dating of scarpsformed by repeated slip events along the San Andreas Fault, Carrizo Plain. Calif. J. Geophys. Res. 103, 10141–10160.
Bashmachnikov, I., Loureiro, C., Martins, A., 2013. Topographically induced circulation patterns and mixing over Condor seamount. Deep-Sea Res. II Top. Stud. Oceanogr. 98, 38–51.
Beier, C., Haase, K.M., Abouchami, W., 2015. Geochemical and geochronological constraints on the volcanic evolution of the Azores Plateau. Geol. Soc. Am. Spec. Pap. 5111, 27–55.
Beier, C., Bach, W., Blum, M., Cerqueira, T., Ferreira, P.J., Genske, F.S., Haase, K.M., Kausche, A.H., Kemner, F., Klügel, A., Krumm, S.H., Kueppers, U., Leymann, T., Mai, A., Petry, F., Ratmeyer, V., Raeke, A., Rentsch, H., Romer, R.H.W., Sampaio, I., Schade, T., Schleifer, B., Schröder, M.K., Skambraks, T.O., Storch, B., Vittori, V.F., Wefer, G., 2017. Azores Plateau – Cruise No. M128 – July 2 – July 27, 2016 - Ponta Delgada (Azores, Portugal) – Ponta Delgada (Azores, Portugal). University of Bremen, Bremen, Germany.
Bintanja, R., van de Wal, R.S.W., 2008. North American ice-sheet dynamics and the onset of 100,000-year glacial cycles. Nature 454, 869–872.
Blondel, P., Murton, B.J., 1997. Interpretation of Sidescan Sonar Imagery. John Wiley, Chichester, p. 317.
Candio, S., Gillespie, T., Wilkins, C.C., Morrow, T., Cantwell, K., 2022. Mapping data acquisition and processing summary report: EX-22-06: voyage to the ridge 3 (ROV and mapping). National Oceanographic and Atmospheric Administration, Silver Spring, Maryland, USA.
Carrilho, F., Custódio, S., Bezzeghoud, M., Oliveira, C.S., Marreiros, C., Vales, D., Alves, P., Pena, A., Madureira, G., Escuer, M., Silveira, G., Corela, C., Matias, L., Silva, M., Veludo, I., Dias, N.A., Loureiro, A., Borges, J.F., Caldeira, B., Wachilala, P., Fontiela, J., 2021. The Portuguese National Seismic Network - products and services. Seismol. Res. Lett. 92, 1541–1570.
Casalbore, D., Romagnoli, C., Bosman, A., Chiocci, F.L., 2011. Potential tsunamigenic landslides at Stromboli Volcano (Italy): Insight from marine DEM analysis. Geomorphology 126, 42–50.
Casalbore, D., Romagnoli, C., Pimentel, A., Quartau, R., Casas, D., Ercilla, G., Hipólito, A., Sposato, A., Chiocci, F.L., 2015. Volcanic, tectonic and mass-wasting processes offshore Terceira Island (Azores) revealed by high-resolution seafloor mapping. Bull. Volcanol. 77, 24.
Chadwick, W.W., Cashman, K.V., Embley, R.W., Matsumoto, H., Dziak, R.P., de Ronde, C. E.J., Lau, T.K., Deardorff, N.D., Merle, S.G., 2008a. Direct video and hydrophone observations of submarine explosive eruptions at NW Rota-1 volcano, Mariana arc. J. Geophys. Res. 113, B08S10. https://doi.org/10.1029/2007JB005215.
Chadwick, W.W.J., Wright, I.C., Schwartz-Schampera, U., Hyvernaud, O., Reymond, D., de Ronde, C.E.J., 2008b. Cyclic eruptions and sector collapses at Monowai submarine volcano, Kermadec arc: 1998-2007. Geochem. Geophys. Geosyst. 9, Q10014. https://doi.org/10.11029/12008GC002113.
Chandler, R.J., 1973. The inclination of talus: Arctic talus terraces and other slopes composed of granular material. J. Geol. 81, 1–14.
Chang, Y.-C., Mitchell, N.C., Quartau, R., 2021. Landslides in the upper submarine slopes of volcanic islands: the Central Azores. Geochem. Geophys. Geosyst. 22, e2021GC009833.
Chang, Y.-C., Mitchell, N.C., Shingles-Belo, J.C., Hansteen, T.H., Freundt, A., Hübscher, C., Quartau, R., 2023. Emplacement history of volcaniclastic turbidites around the Central Azores volcanic islands: Frequencies of slope landslides and eruptions. Geosphere 19, 654–675. https://doi.org/10.1130/GES02570.02571.
Chiocci, F.L., Romagnoli, C., Bosman, A., 2008a. Morphologic resilience and depositional processes due to rapid evolution of the submerged Sciara del Fuoco (Stromboli Island) after the December 2002 submarine slide and tsunami. Geomorph 100, 356–365.
Chiocci, F.L., Romagnoli, C., Tommasi, P. and Bosman, A., 2008b. The Stromboli 2002 tsunamigenic submarine slide: Characteristics and possible failure mechanism. J. Geophys. Res., 113: art. B10102, doi:10.11029/12007JB005172.
Collico, S., Arroyo, M., Urgeles, R., Gràcia, E., Devincenzi, M., Peréz, N., 2020. Probabilistic mapping of earthquake-induced submarine landslide susceptibility in the South-West Iberian margin. Mar. Geol. 429, 106296.
de Moustier, C., 1988. State of the art in swath bathymetry survey systems. Int. Hydr. Rev. Monaco 65 (2), 25–54.
de Moustier, C., Kleinrock, M.C., 1986. Bathymetric artifacts in Sea Beam data: how to recognize them and what causes them. J. Geophys. Res. 91, 3407–3424.
Densmore, A.L., Anderson, R.S., McAdoo, B.G., Ellis, M.A., 1997. Hillslope evolution by bedrock landslides. Science 275, 369–372.
Escartín, J., Leclerc, F., Olive, J.-A., Mevel, C., Cannat, M., Petersen, S., Augustin, N., Feuillet, N., Deplus, C., Bezos, A., Bonnemains, D., Chavagnac, V., Choi, Y., Godard, M., Haaga, K.A., Hamelin, C., Ildefonse, B., Jamieson, J.W., John, B.E., Leleu, T., MacLeod, C.J., Massot-Campos, M., Nomikou, P., Paquet, M., Rommevaux-Jestin, C., Rothenbeck, M., Steinführer, A., Tominaga, M., Triebe, L., Campos, R., Gracias, N., Garcia, R., Andreani, M., Vilaseca, G., 2016. First direct observation of coseismic slip and seafloor rupture along a submarine normal fault and implications for fault slip history. Earth Planet. Sci. Lett. 450, 96–107.
Flewellen, C., Millard, N., Rouse, I., 1993. TOBI, a vehicle for deep ocean survey. J. Elect. Comm. Eng. 85–93.
Fornari, D.J., Moore, J.G., Calk, L., 1979. A large submarine sand-rubble flow on Kilauea volcano, Hawaii. Volcanol. Geotherm. Res. 5, 239–256.
Freire Luis, J., Miranda, J.M., Galdeano, A., Patriat, P., Rossignol, J.C., Victor, L.A.M., 1994. The Azores triple junction evolution since 10 Ma from an aeromagnetic survey of the Mid-Atlantic Ridge. Earth Planet. Sci. Lett. 125, 439–459.
Gente, P., Dyment, J., Maia, M., Goslin, J., 2003. Interaction between the Mid-Atlantic Ridge and the Azores hot spot during the last 85 Myr: Emplacement and rifting of the hot spot-derived plateaus. Geochem. Geophys. Geosyst. 4, 8514. https://doi.org/10.1029/2003GC000527.
Goldfinger, C., Nelson, C.H., Johnson, J.E., 2003. Holocene earthquake records from the Cascadia subduction zone and northern San Andreas Fault based on precise dating of offshore turbidites. Annu. Rev. Earth Planet. Sci. 31, 555–577.
Gray, H.J., Mahan, S.A., Rittenour, T.M., Nelson, M.S., 2015. Guide to luminescence dating techniques and their application for paleoseismic research. In: Lund, W.R. (Ed.), Proceedings volume: Basin and Range province seismic hazards summit III, 2015 (Utah Geological Survey Miscellaneous Publication 15–5). Utah Geological Survey, Salt Lake City, UT, p. 18.
Hampton, M.A., Lee, H.J., Locat, J., 1996. Submarine landslides. Rev. Geophys. 34, 33–59.
Hübscher, C., et al., 2015. Azores Plateau, Cruise No. M113/1 December 29, 2014 - January 22, 2015. Ponta Delgada (Portugal) - Ponta Delgada (Portugal), Bremen.
Hübscher, C., Beier, C., Al-Hseinat, M., Batista, L., Blum, M., Bobsin, M., Bülow, J., Frahm, L., Grob, H., Hildenbrandt, A., Kalvelage, C., Kammann, J., Knevels, K., Levanos, I., Nomikou, P., Reichel, H., Petry, F., Spickermann, D., Stackemann, F., Stratmann, S., Terrinha, P., Vögele, M., Winter, S., Schaaf, T., Schleifer, B., Stelzner, M., Spitzy, A., Weinzierl, C., Weiß, B., 2016. Azores Plateau – Cruise No. M113/1 – December 29, 2014 – January 22, 2015 – Ponta Delgada (Portugal) – Ponta Delgada (Portugal). University of Bremen, Bremen, Germany.
Hughes Clarke, J.E., Mayer, L.A., Wells, D.E., 1996. Shallow-water imaging multibeam sonars: a new tool for investigating seafloor processes in the coastal zone and on the continental shelf. Mar. Geophys. Res. 18, 607–629.
Hughes, A., Escartín, J., Billant, J., Leclerc, F., Andreani, M., Olive, J.-A., Arnaubec, A., Dano, A., Delorme, A., Deplus, C., Feuillet, N., Gini, C., Gracias, N., Hamelin, C., Istenic, K., Komorowski, J.-C., Le Friant, A., Marchand, C., Mével, C., Onstad, S.L., Quidelleur, X., 2023. Seafloor earthquake ruptures and mass wasting from the 2004 Mw 6.3 Les Saintes submarine earthquake. Comm. Earth Environ. 4, 270.
Kauahikaua, J.P., Denlinger, R., Foster, J., Keszthelyi, L., 1993. Lava delta instability: is it mass-wasting or is it triggered by lava flowing through tubes? EOS Trans. AGU 74, 616.
Kenter, J.A.M., Schlager, W., 1989. A comparison of shear strength in calcareous and siliclastic marine sediments. Mar. Geol. 88, 145–152.
Leclerc, F., Palagonia, S., Feuillet, N., Nomikou, P., Lampridou, D., Barrière, P., Dano, A., Ochoa, E., Gracias, N., Escartin, J., 2024. Large seafloor rupture caused by the 1956 Amorgos tsunamigenic earthquake, Greece. Comm. Earth Environ. 5, 663.

Lee, H.J., Torresan, M.E., McArthur, W., 1994. Stability of submerged slopes on the flanks of the Hawaiian Islands, a simplified approach. Open-File Rep. 94-638, 1–54.
Lee, H.J., Greene, H.G., Edwards, B.D., 2009. Submarine landslides of the Southern California Borderland. In: Lee, H.J., Normark, W.R. (Eds.), Earth Science in the Urban Ocean: The Southern California Continental Borderland: Geological Society of America Special Paper 454. Geological Society of America, pp. 251–269.
Ligi, M., Mitchell, N.C., Marani, M., Gamberi, F., Penitenti, D., Carrara, G., Rovere, M., Portaro, R., Centorami, G., Bortoluzzi, G., Jacobs, C., Rouse, I., Flewellen, C., Whittle, S., Terrinha, P., Freire Luis, J., Lourenco, N., 1999. Giant volcanic ridges amongst the Azores islands. EOS Trans. (AGU, 80, Fall Meet. Suppl.: F913).
Lourenço, N., Miranda, J.M., Luis, J.F., Ribeiro, A., Victor, L.A.M., Madeira, J., Needham, H.D., 1998. Morpho-tectonic analysis of the Azores volcanic plateau from a new bathymetric compilation of the area. Mar. Geophys. Res. 20, 141–156.
Luis, J., Lourenço, N., Mata, J., Madureira, P., Goslin, J., Perrot, J., Brachet, C., Simão, N., 2006. The "STRIPAREA" cruise: highly detailed multibeam bathymetry survey of Azores Triple Junction area. InterRidge News 15, 16–18.
Madeira, J., Brum da Silveira, A., 2003. Active tectonics and first paleoseismological results in Faial, Pico and S. Jorge islands (Azores, Portugal). Ann. Geophys. 46, 733–761.
Madeira, J., Brum da Silveira, A., Hipólito, A., Carmo, R., 2015. Active tectonics in the central and eastern Azores islands along the Eurasia-Nubia boundary: a review. In: Gaspar, J.L., Guest, J.E., Duncan, A.M., Barriga, F.J.A.S., Chester, D.K. (Eds.), Volcanic Geology of São Miguel Island (Azores Archipelago), vol. 44. Geological Society, London, pp. 15–32.
Marques, F.O., Catalão, J.C., DeMets, C., Costa, A.C.G., Hildenbrand, A., 2013. GPS and tectonic evidence for a diffuse plate boundary at the Azores Triple Junction. Earth Planet. Sci. Lett. 381, 177–187.
Masson, D.G., Watts, A.B., Gee, M.J.R., Urgeles, R., Mitchell, N.C., Le Bas, T.P., 2002. Slope failures on the flanks of the western Canary Islands. Earth Sci. Rev. 57, 1–35.
Matias, L., Dias, N.A., Morais, I., Vales, D., Carrilho, F., Madeira, J., Gaspar, J.L., Senos, L., Silveira, A.B., 2007. The 9th of July 1998 Faial Island (Azores, North Atlantic) seismic sequence. J. Seismol. 11, 275–298.
McNutt, S.R., 1996. Seismic monitoring and mruption forecasting of volcanoes: A review of the state-of-the-art and case histories. In: Scarpa, R., Tilling, R.I. (Eds.), Monitoring and Mitigation of Volcanic Hazards. Springer, Berlin, pp. 99–146.
Mezcua, J., Blanco, R.M.G., Rueda, J., 2008. On the strong ground motion attenuation in Spain. Bull. Seismol. Soc. Am. 98, 1343–1353.
Miranda, J.M., Luis, J.F., Lourenço, N., Goslin, J., 2014. Distributed deformation close to the Azores Triple "Point". Mar. Geol. 355, 27–35.
Miranda, J.M., Luis, J.F., Lourenço, N., Fernandes, R.M.S., 2015. The structure and evolution of the Azores Triple Junction: Implications for S. Miguel Island. In: Gaspar, J.L., Guest, J.E., Duncan, A.M., Barriga, F.J.A., Chester, D.K. (Eds.), Volcanic Geology of São Miguel Island (Azores Archipelago). Geol. Soc. London, London, pp. 5–13.
Mitchell, N.C., 1993. A model for attenuation of backscatter due to sediment accumulations and its application to determine sediment thickness with GLORIA sidescan sonar. J. Geophys. Res. 98, 22477–22493.
Mitchell, N.C., 1996a. Creep in pelagic sediments and potential for morphologic dating of marine fault scarps. Geophys. Res. Lett. 23 (5), 483–486.
Mitchell, N.C., 1996b. Processing and analysis of Simrad multibeam sonar data. Mar. Geophys. Res. 18, 729–739.
Mitchell, N.C., 2021. Seamounts. In: Shroder, J.J.F. (Ed.), Treatise on Geomorphology, vol. 8. Elsevier, Academic Press, pp. 901–918. https://doi.org/10.1016/B978-0-12-818234-5.00102-4.
Mitchell, N.C., Somers, M.L., 1989. Quantitative backscatter measurements with a long range side-scan sonar. IEEE J. Ocean. Eng. 14, 368–374.
Mitchell, N.C., Tivey, M.A., Gente, P., 2000. Slopes of mid-ocean ridge fault scarps from submersible observations. Earth Planet. Sci. Lett. 183, 543–555.
Mitchell, N.C., Beier, C., Rosin, P., Quartau, R., Tempera, F., 2008. Lava penetrating water: Submarine lava flows around the coasts of Pico Island, Azores. Geochem. Geophys. Geosyst. 9, Q03024. https://doi.org/10.01029/02007GC001725.
Mitchell, N.C., Stretch, R., Oppenheimer, C., Kay, D., Beier, C., 2012. Cone morphologies associated with shallow marine eruptions: East Pico Island. Azores. Bull. Volcanol. 74, 2289–2300.
Mitchell, N.C., Stretch, R., Tempera, F., Ligi, M., 2018. Volcanism in the Azores: A marine geophysical perspective. In: Beier, C., Küppers, U. (Eds.), Volcanoes of the Azores. Springer Publications, pp. 101–126. https://doi.org/10.1007/1978-1003-1642-32226-32226_32227.
Mohn, C., Hansen, J.L.S., Carreiro-Silva, M., Cunningham, S.A., de Froe, E., Dominguez-Carrió, C., Gary, S., Glud, R.N., Göke, C., Johnson, C., Morato, T., Møller, E.F., Rovelli, L., Schulz, K., Soetaert, K., van der Kaaden, A., van Oevelen, D., 2023. Tidal to decadal scale hydrodynamics at two contrasting cold-water coral sites in the Northeast Atlantic. Prog. Oceanogr. 214, 103031.
Moore, J.G., Clague, D.A., Holcomb, R.T., Lipman, P.W., Normark, W.R., Torresan, M.E., 1989. Prodigious submarine landslides on the Hawaiian Ridge. J. Geophys. Res. 94, 17465–17484.
Moore, J.G., Normark, W.R., Holcomb, R.T., 1994. Giant Hawaiian landslides. Annu. Rev. Earth Planet. Sci. 22, 119–144.
Morgenstern, N.R., 1967. Submarine slumping and the initiation of turbidity currents. In: Richards, A.F. (Ed.), Marine Geotechnique. Univ. of Ill. Press, Urbana, pp. 189–210.
Murton, B.J., Rouse, I., Millard, N.W., Flewellen, C., 1992. Multisensor, deep-towed instrument explores ocean floor. EOS Trans. Am. Geophys. Union 73, 225–227.
Neves, M.C., Miranda, J.M., Luis, J.F., 2013. The role of lithospheric processes on the development of linear volcanic ridges in the Azores. Tectonophysics 608, 376–388.
Nieminski, N.M., Sylvester, Z., Covault, J.A., Gomberg, J., Staisch, L., McBrearty, I.W., 2024. Turbidite correlation for paleoseismology. Geol. Soc. Am. Bull. https://doi.org/10.1130/B37343.1.
Omira, R., Quartau, R., Ramalho, I., Baptista, M.A., Mitchell, N.C., 2016. The tsunami effects of a collapse of a volcanic island on a semienclosed basin: the Pico-São Jorge Channel in the Azores Archipelago. In: Duarte, J.C., Schellart, W.P. (Eds.), Plate Boundaries and Hazards, Geophys. Monogr. 219. American Geophysical Union and John Wiley & Sons, pp. 271–287.
Pritchard, M.E., Mather, T.A., McNutt, S.R., Delgado, F.J., Reath, K., 2018. Thoughts on the criteria to determine the origin of volcanic unrest as magmatic or non-magmatic. Philos. Trans. R. Soc. A377, 20180008.
Quartau, R., Hipólito, A., Romagnolii, C., Casalbore, D., Madeira, J., Tempera, F., Roque, C., Chiocci, F.L., 2014. The morphology of insular shelves as a key for understanding the geological evolution of volcanic islands: insights from Terceira Island (Azores). Geochem. Geophys. Geosyst. 15. https://doi.org/10.1002/2014GC005248.
Rampello, S., Callisto, L., Fargnoli, P., 2010. Evaluation of slope performance under earthquake loading conditions. Ital. Magaz. Geotech. 4, 30–41.
Romer, R.H.W., Beier, C., Haase, K.M., Hübscher, C., 2018. Correlated changes between volcanic structures and magma composition in the Faial volcanic system, azores. Front. Earth Sci. 6, 78.
Ryan, W.B.F., Carbotte, S.M., Coplan, J.O., O'Hara, S., Melkonian, A., Arko, R., Wiessel, R.A., Ferrini, V., Goodwillie, A., Nitsche, F., Bonczkowski, J., Zemsky, R., 2009. Global multi-resolution topography synthesis. Geochem. Geophys. Geosyst. 10, Q03014.
Sawyer, D.E., DeVore, J.R., 2015. Elevated shear strength of sediments on active margins: evidence for seismic strengthening. Geophys. Res. Lett. 42, 10216–10221.
Schindelé, F., Kong, L., Lane, E.M., Paris, R.L., Ripepe, M., Titov, V., Bailey, R., 2024. A Review of Tsunamis Generated by Volcanoes (TGV) Source Mechanism, Modelling, monitoring and Warning Systems. Pure Appl. Geophys. 181, 1745–1792.
Schmitt, T., Mitchell, N.C., Ramsay, A.T.S., 2008. Characterizing uncertainties for quantifying bathymetry change between time-separated multibeam echo-sounder surveys. Cont. Shelf Res. 28, 1166–1176.
Schwab, W.C., Lee, H.J., 1988. Causes of two slope-failure types in continental shelf sediment, northeastern Gulf of Alaska. J. Sediment. Petrol. 58, 1–11.
Smith, D.K., Kong, L.S.L., Johnson, K.T.M., Reynolds, J.R., 2002. Volcanic morphology of the submarine Puna Ridge, Kilauea volcano. In: Takahashi, E., Lipman, P.W., Garcia, M.J., Naka, J., Aramaki, S. (Eds.), Hawaiian Volcanoes, Deep Underwater Perspectives. American Geophysical Union, Washington, DC, pp. 125–142.
Stretch, R., Mitchell, N.C., Portaro, R.A., 2006. A morphometric analysis of the submarine volcanic ridge of Pico Island. J. Volcanol. Geotherm. Res. 156, 35–54.
Tempera, F., Giacomello, E., Mitchell, N.C., Campos, A.S., Henriques, A.B., Martins, A., Bashmachnikov, I., Mendonça, A., Morato, T., Colaço, A., Porteiro, F.M., Catarino, D., Gonçalves, J., Pinho, M.R., Isidro, E.J., Santos, R.S., Menezes, G., 2012. Mapping the Condor seamount seafloor environment and associated biological assemblages (Azores, NE Atlantic). In: Harris, P.T., et al. (Eds.), Seafloor Geomorphology as Benthic Habitat: Geohab Atlas of Seafloor Geomorphic Features and Benthic Habitats. Elsevier, London, pp. 807–818.
Tempera, F., Hipólito, A., Madeira, J., Vieira, S., Campos, A.S., Mitchell, N.C., 2013. Condor seamount (Azores, NE Atlantic): a morpho-tectonic interpretation. Deep-Sea Res. II Top. Stud. Oceanogr. 98, 7–23.
ten Brink, U.S., Barkan, R., Andrews, B.D., Chaytor, J.D., 2009. Size distribution and failure initiation of submarine and subaerial landslides. Earth Planet. Sci. Lett. 287, 31–42.
ten Brink, U.S., Andrews, B., Miller, N., 2016. Seismicity and sedimentation rate effects on submarine slope stability. Geology 44, 563–566.
Tepp, G., Dziak, R.P., 2021. The seismo-acoustics of submarine volcanic eruptions. J. Geophys. Res. 126, e2020JB020912.
Tinkler, K.J., 1966. Slope profiles and scree in Eglwyseg Valley, North Wales. Geogr. J. 132, 379–385.
Tinti, S., Manucci, A., Pagnoni, G., Armigliato, A., Zaniboni, F., 2005. The 30 December 2002 landslide-induced tsunamis in Stromboli: sequence of events reconstructed from the eyewitness accounts. Nat. Hazards Earth Syst. Sci. 5, 763–775.
Tinti, S., Pagnoni, G., Zaniboni, F., 2006. The landslides and tsunamis of the 30th of December 2002 in Stromboli analysed through numerical simulations. Bull. Volcanol. 68, 462–479.
Tucker, M.E., Carey, S.N., Sparks, R.S.J., Stinton, A., Leng, M., Robinson, L., Li, T., Lewis, J., Cotton, L., 2020. Carbonate crusts around volcanic islands: Composition, origin and their significance in slope stability. Mar. Geol. 429, 106320.
van der Kooij, B., Immenhauser, A., Steuber, T., Bahamonde, J.R., Merino Tomé, O., 2010. Precipitation mechanisms of volumetrically important early marine carbonate cement volumes in deep-slope settings. Sedimentology 57, 1491–1525.
Vogt, P.R., Jung, W.Y., 2004. The Terceira Rift as a hyper-slow, hotspot-dominated oblique spreading axis: a comparison with other slow-spreading plate boundaries. Earth Planet. Sci. Lett. 218, 77–90.
Wallace, R.E., 1977. Profiles and ages of young fault scarps, north Central Nevada. Bull. Geol. Soc. Am. 88, 1267–1281.
Ward, S.N., Day, S., 2001. Cumbre Vieja Volcano – Potential collapse and tsunami at La Palma, Canary Islands. Geophys. Res. Lett. 28, 3397–3400.
Watts, A.B., Masson, D.G., 1995. A giant submarine slide on the north flank of Tenerife, Canary Islands. J. Geophys. Res. 100, 24,487–24,498.
Watts, A.B., Masson, D.G., 2001. New sonar evidence for recent catastrophic collapses of the north flank of Tenerife, Canary Islands. Bull. Volcanol. 63, 8–19.
Weiß, B.J., Hübscher, C., Wolf, D., Lüdmann, T., 2015. Submarine explosive volcanism in the southeastern Terceira Rift/São Miguel region (Azores). J. Volcanol. Geotherm. Res. 303, 79–91.

Wessel, P., Smith, W.H.F., 1991. Free software helps map and display data. EOS Trans. Am. Geophys. Union 72, 441.
Wessel, P., Luis, J.F., Uieda, L., Scharroo, R., Wobbe, F., Smith, W.H.F., Tian, D., 2019. The generic mapping tools version 6. Geochem. Geophys. Geosyst. 20, 5556–5564.
Winters, W.J., Lee, H.J., 1982. Evaluation of Geotechnical Properties and Slope Stability of Calcareous Ooze on the South-West Slope off Oahu, Hawaii, USGS Open-File Report 82-468B. USGS, Menlo Park, California.
Wisshak, M., Berning, B., Jakobsen, J., Freiwald, A., 2015. Temperate carbonate production: biodiversity of calcareous epiliths from intertidal to bathyal depths (Azores). Mar. Biodivers. 45, 87–112.
Zeppilli, D., Bongiorni, L., Cattaneo, A., Danovaro, R., Santos, R.S., 2013. Meiofauna assemblages of the Condor Seamount (North-East Atlantic Ocean) and adjacent deep-sea sediments. Deep-Sea Res. II 98, 87–100.